Title

Re-anchoring the late Pleistocene tephrochronology of New Zealand based on concordant radiocarbon ages and combined $^{238}U/^{230}Th$ disequilibrium and (U—Th)/He zircon ages

Authors

Danišík, Martin
Shane, Phil
Schmitt, Axel K
et al.

Publication Date

2012-10-01

DOI

10.1016/j.epsl.2012.06.041

Peer reviewed

Earth and Planetary Science Letters 349–350 (2012) 240–250

Contents lists available at SciVerse ScienceDirect

Earth and Planetary Science Letters

journal homepage: www.elsevier.com/locate/epsl

Re-anchoring the late Pleistocene tephrochronology of New Zealand based on concordant radiocarbon ages and combined $^{238}U/^{230}Th$ disequilibrium and (U–Th)/He zircon ages

Martin Danišík [a,b,*], Phil Shane [c], Axel K. Schmitt [d], Alan Hogg [e], Guaciara M. Santos [f], Sonja Storm [c], Noreen J. Evans [b,g], L. Keith Fifield [h], Jan M. Lindsay [c]

[a] Department of Earth and Ocean Sciences, The University of Waikato, Private Bag 3105, Hamilton 3240, New Zealand
[b] John de Laeter Centre for Isotope Research, Applied Geology, Curtin University of Technology, GPO Box U1987, Perth WA 6845, Australia
[c] School of Environment, University of Auckland, Private Bag 92019, Auckland 1010, New Zealand
[d] Department of Earth and Space Sciences, University of California Los Angeles, 595 Charles Young Drive E, Los Angeles CA 90095, USA
[e] Radiocarbon Laboratory, University of Waikato, Private Bag, Hamilton, New Zealand
[f] Keck-CCAMS Group Earth System Science Department, University of California, Irvine, CA 92697-3100, USA
[g] CSIRO Earth Science and Resource Engineering, ARRC, 26 Dick Perry Avenue, WA 6151, Australia
[h] Department of Nuclear Physics, Research School of Physical Sciences and Engineering, Australian National University, Canberra ACT 0200, Australia

ARTICLE INFO

Article history:
Received 12 February 2012
Received in revised form
12 June 2012
Accepted 22 June 2012
Editor: L. Stixrude
Available online 14 August 2012

Keywords:
$^{238}U/^{230}Th$ disequilibrium dating
(U–Th)/He dating
radiocarbon dating
Quaternary geochronology
Rotoiti eruption
Taupo Volcanic Zone

ABSTRACT

The caldera-forming Rotoiti eruption from Okataina volcano was one of the largest rhyolite events of the last 100 ka in the Taupo Volcanic Zone, New Zealand. Its associated widespread tephra layer (Rotoehu tephra) is a significant time marker in terrestrial–marine paleoclimate correlation studies in the SW Pacific. However, the accurate and precise age of this eruption, and of the subsequent, smaller volume Earthquake Flat (EQF) eruption, has been the subject of controversy despite numerous studies. We have applied combined $^{238}U/^{230}Th$ disequilibrium and (U–Th)/He dating of zircon from Rotoiti and EQF deposits, and obtained overlapping ages of $45.1(7) \pm 3.3$ ka and $45.1(6) \pm 2.9$ ka, respectively. These results are supported by new and published high-precision radiocarbon data bracketing the age of the Rotoiti eruption between 44.8 ± 0.3 and 47.5 ± 2.1 ka cal BP. These age data are also in good agreement with a range of previously published estimates based on paleoclimate (palynology), luminescence dating of enclosing sediment, and sedimentation rates in terrestrial and marine settings. However, these results are at variance with a commonly quoted age of ~60 ka, largely constrained by a single $^{40}Ar/^{39}Ar$ age of an overlying glassy lava flow at a distal tephra site. This study demonstrates the potential for combined $^{238}U/^{230}Th$ disequilibrium and (U–Th)/He dating of zircon in tephra and other volcanic deposits to provide age control in the 40–100 ka time interval, a period difficult to constrain using more traditional radiocarbon, K/Ar and $^{40}Ar/^{39}Ar$ methods.

1. Introduction

K/Ar, $^{40}Ar/^{39}Ar$ and radiocarbon (^{14}C) methods are the chief chronological approaches for constraining the age of young volcanic deposits. However, these methods are often severely limited by (1) the scarcity of materials suitable for dating (e.g., the absence of high-K mineral phases, such as sanidine, or associated organic material for ^{14}C dating); (2) open-system behaviour of radioactive parent–daughter pairs (e.g., mobility of K and Ar in glasses, or excess ^{40}Ar; Chen et al., 1996; McDougall and Harrison, 1998; Spell et al., 2001); (3) mass-dependent kinetic isotopic fractionation (e.g., for Ar dating of obsidian; Morgan et al., 2009); and (4) limitations in analytical sensitivity (e.g., low radiogenic daughter yields, or exhaustion of short-lived radioactive parents). In addition, the presence of undetected xenocrysts can produce erroneous K/Ar and $^{40}Ar/^{39}Ar$ results (e.g., Walter et al., 1991). For ^{14}C dating, the uncertainties in the calibration curve, due to too few and comparatively imprecise calibration points in the age range ~40–50 ka (Reimer et al., 2009), detrimentally affect the accuracy of ^{14}C ages.

(U–Th)/He dating of zircon (e.g., Farley et al., 2002; Reiners et al., 2004; Blondes et al., 2007), especially when combined with $^{238}U/^{230}Th$ disequilibrium dating (e.g., Schmitt et al., 2006), has the potential to fill a critical gap in Quaternary chronology particularly in a time-window between ~50 and 300 ka that is

* Corresponding author at: Department of Earth and Ocean Sciences, The University of Waikato, Private Bag 3105, Hamilton 3240, New Zealand.
Tel.: +64 7 8585163; fax: +61 7 8560115.
E-mail address: M.Danisik@waikato.ac.nz (M. Danišík).

0012-821X/$ - see front matter © 2012 Elsevier B.V. All rights reserved.
http://dx.doi.org/10.1016/j.epsl.2012.06.041

difficult to access by conventional chronometers, and the lower end of which is close to or beyond the ^{14}C dating limit (Reimer et al., 2009). Moreover, zircon is a common accessory mineral in silicic rocks, albeit scarce in mafic rocks. The (U–Th)/He system is characterized by fast diffusion of the radiogenic daughter ^{4}He, thus minimizing the effect of pre-eruptive ^{4}He in magmatic xeno- or antecrysts. The U–Th decay systems are intrinsically sensitive due to rapid accumulation of ^{4}He (~20-times faster than ^{40}Ar per parent nucleus) coupled with low backgrounds (atmospheric ^{4}He being 2000 times lower than ^{40}Ar; Farley, 2002).

To explore the potential of combined $^{238}U/^{230}Th$ disequilibrium and (U–Th)/He dating of zircon in the ~50–300 ka window, we focused on the pyroclastic deposits of the Rotoiti and Earthquake Flat (EQF) eruptions in the Taupo Volcanic Zone (TVZ) of New Zealand (Fig. 1) which are thought to have been produced during this time period. The Rotoiti eruption was one of the largest (~100 km^3 of magma) TVZ eruptions in the last 100 ka, and was associated with caldera collapse in the Okataina Volcanic Centre (OVC) (Nairn, 2002). The smaller EQF eruption (~5–10 km^3 of magma) erupted from Kapenga volcano, about 25 km SW of the assumed Rotoiti vent. Deposits of the EQF eruption conformably overlie those of the Rotoiti, without any sign of erosion or weathering suggesting a time break of only weeks-months (Nairn and Kohn, 1973). The Rotoiti fall deposits (Rotoehu tephra) underpin the tephrochronological record of well-dated and mapped tephra layers in New Zealand (Shane, 2000; Lowe, 2011), and hence provide an important chronological constraint for the frequency of eruptions. The Rotoehu tephra is also a key horizon in the correlation of Last Glacial paleoenvironmental changes between the marine and terrestrial realms (Shane and Sandiford, 2003; Wilson et al., 2007), and is found >1000 km from its source in the Pacific Ocean (Allan et al., 2008).

Previous attempts to date the Rotoiti and EQF eruptions exemplify common failures of producing concordant ages by various direct and indirect chronological techniques that have included isotopic, radiometric, radiation exposure, and stratigraphic approaches (see

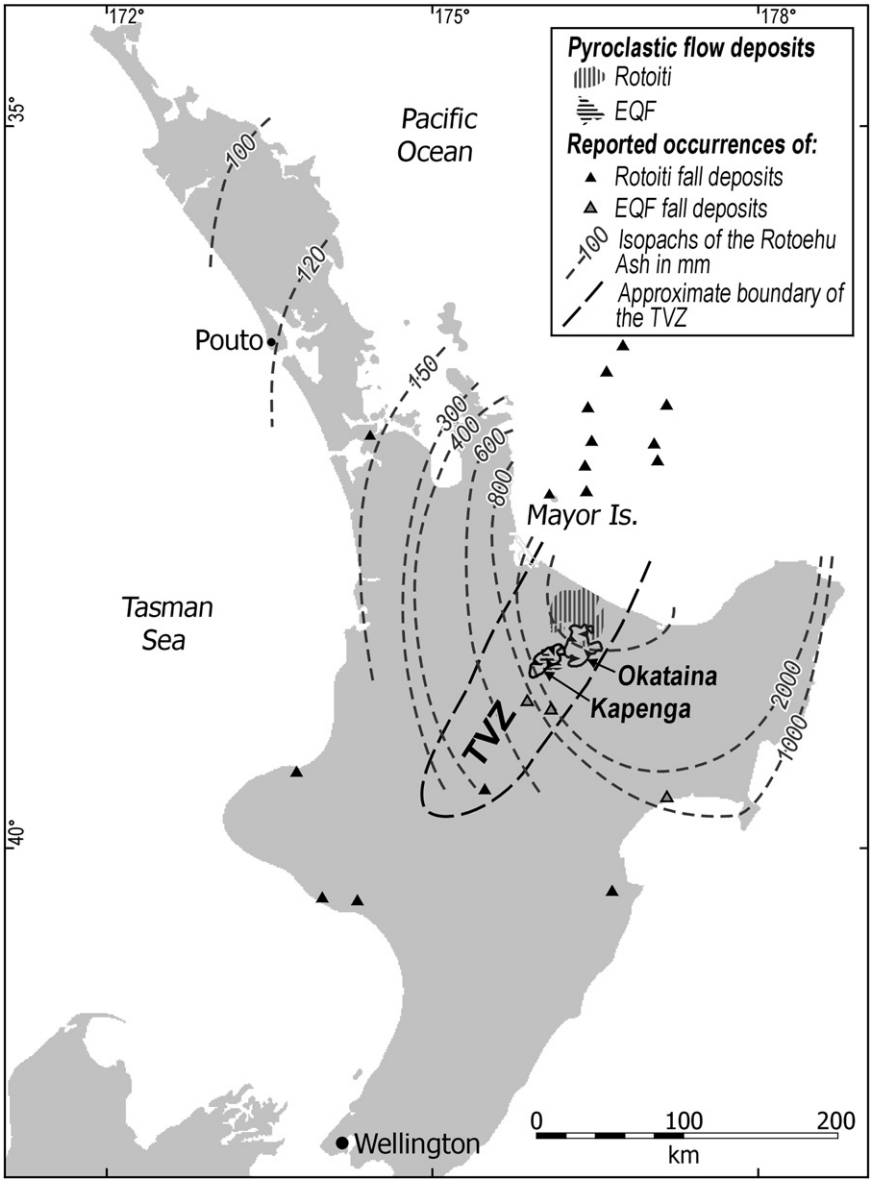

Fig. 1. Simplified map of North Island, New Zealand, showing the distribution of pyroclastic flow (horizontal and vertical hatching) and fall deposits (isopachs and triangles) from the Rotoiti and EQF eruptions, which originated from Okataina and Kapenga volcanic centres in the Taupo Volcanic Zone (TVZ), respectively (On-land data from Nairn and Kohn, 1973; Pullar and Birrell, 1973; Nairn, 2002; Shane and Sandiford, 2003; Molloy et al., 2009; Off-shore data from Shane et al., 2006). In addition, ODP site 1123 (41°47.160S, 171°29.940E, not shown in the figure) with the Rotoehu tephra (Allan et al., 2008) is located ~1000 km east of New Zealand.

summaries in Froggatt and Lowe, 1990; Lowe and Hogg, 1995; Shane and Sandiford, 2003; Wilson et al., 2007). Among these data is a frequently cited 61.0 ± 1.4 ka eruption age that is based on K/Ar and $^{40}Ar/^{39}Ar$ ages of glassy lava bracketing the Rotoehu tephra at a distal site (Wilson et al., 2007). However, paleoclimatic and sedimentological studies of maar sediments point to a post-50 ka age (e.g., Molloy et al., 2009). Here, we show that combined $^{238}U/^{230}Th$ disequilibrium and (U–Th)/He zircon dating from proximal pumice, along with new ^{14}C ages on wood deposits above and below Rotoehu tephra, place the age of both eruptions > 10 ka younger than the commonly cited ~60 ka age. The ^{14}C ages provide an independent constraint for the zircon-based eruption age, demonstrating the accuracy of the latter and cross-validating both methods.

2. Samples and analytical techniques

2.1. Sample sites

Pumice clasts (10–20 cm in size) were collected from proximal sections of pyroclastic flows formed during the Rotoiti eruption that have previously been the subject of petrological studies (Shane et al., 2005; Molloy et al., 2008). The samples were collected from near the middle of an exposure on Maungarangi Road (sample 559 in Shane et al., 2005) at 37°53′05″S; 176°21′14.3″E, where it comprises at least 5 m of massive, poorly-sorted ignimbrite. The ignimbrite displays incipient vapour-phase alteration. The lower contact is not exposed, and the upper contact represents the top of the widespread pyroclastic flow depositional fan, overlain by ~1–2 m of post-26 ka tephra and paleosols. The pyroclastic fan tapers to the north where flow units become replaced by fine ash beds interbedded with plinian fallout ash and lapilli (Nairn, 2002). At such distal sites, the deposit has been referred to as Rotoehu tephra and correlation is supported by mineralogy and glass chemistry (e.g., Froggatt and Lowe, 1990; Shane et al., 2005).

The EQF pumice was collected from an outcrop on Tumunui Road (38°14′36″S; 176°16′37″E). The sample was collected near the base of a 3 m, crudely stratified, poorly-sorted, non-welded ignimbrite. The lower contact is not exposed, and the upper contact represents the original pyroclastic flow depositional fan surface. This surface is overlain by < 1 m of post-20 ka tephra and paleosols.

Sub-fossil wood above and below Rotoehu tephra was collected from a distal tephra site at Pouto (36°23′32.4″S; 174°07′41.0″E) in northern North Island (Fig. 2A and B), 300 m east of a sample site previously examined by Santos et al. (2001). The site exposes ~28 cm of Rotoehu tephra underlain by 1.1 m of woody lignite over sands. Above the tephra is 2.3 m of woody lignite with seed beds, 1 m of sand, and 1.2 m of woody lignite. The sampled material comprises tree trunks (6–10 cm in diameter) collected 30 and 25 cm above the upper contact of the tephra (samples Pouto 2/3 and 2/4, respectively, Table 1), an epiphyte vine (*Metrosideros robusta*) and a tree trunk collected immediately beneath the lower contact of the tephra (samples Pouto 2/1 and 2/2, Table 1). Growth rings are evident in all four samples.

2.2. $^{238}U/^{230}Th$ disequilibrium dating

Zircon crystals were separated at the University of Auckland from crushed pumice clasts using conventional separation techniques. These included sieving and washing on a Gemini shaking table, heavy liquid and magnetic separation, hand-picking and final leaching in cold 40% HF for 3 min to remove adherent glass from zircon crystals. In order to compare double-dating versus non-double-dating approaches, the zircon concentrates were split into two aliquots. In the first approach, $^{238}U/^{230}Th$ analyses were performed on the zircon followed by (U–Th)/He dating of the same crystals (=double-dating). In the non-double-dating approach, only (U–Th)/He dating was performed on zircons without conducting $^{238}U/^{230}Th$ analysis using average $^{238}U/^{230}Th$ disequilibrium ages for the disequilibrium correction (see below).

$^{238}U/^{230}Th$ disequilibrium analyses on individual zircons were conducted at the University of California Los Angeles (UCLA). Selected zircons were pressed into indium (In) metal with unpolished crystal faces exposed at the surface, coated with a

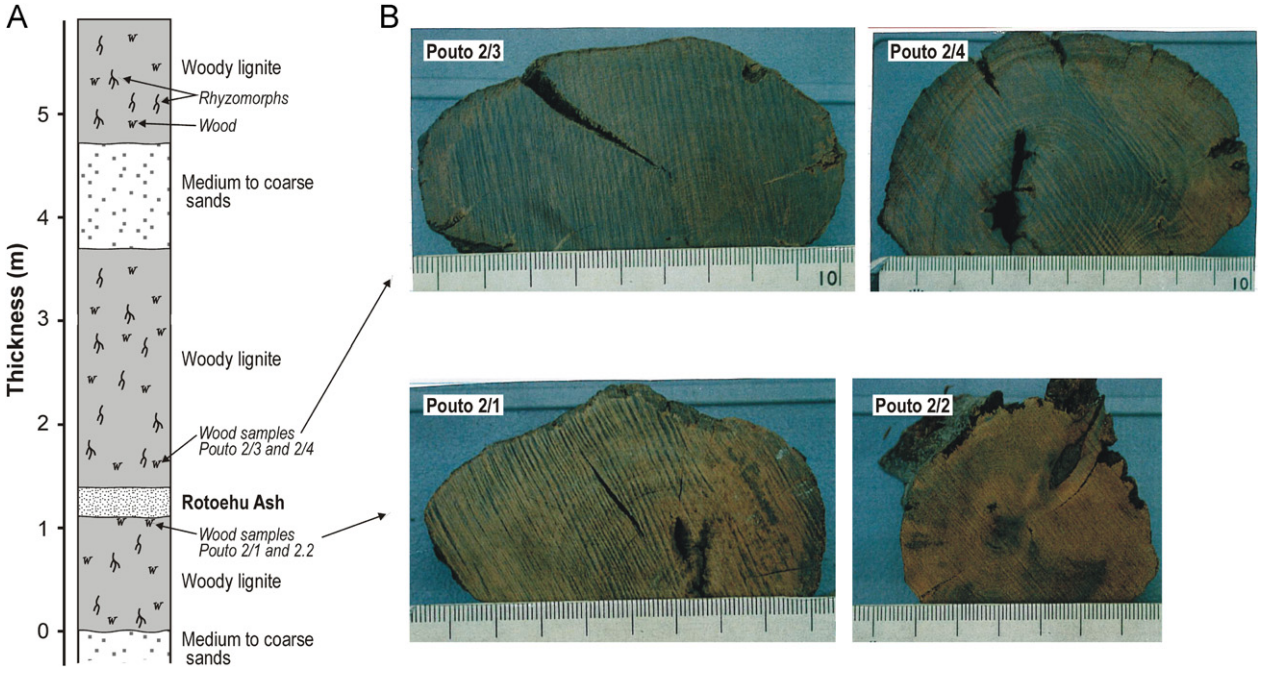

Fig. 2. (A) Schematic stratigraphic column of the Pouto site (for location see Fig. 1) where the wood samples for ^{14}C dating were collected (modified after Alloway, B.V., Pillans, B., Newnham, R.). (B) Photographs of the wood samples used for the ^{14}C dating (scales are in millimetres).

Table 1
^{14}C analytical results.

Sample	Site	Lab no.	Pretreatment/ combustion	δ^{13}C (‰)	^{14}C age $\pm 1\sigma$ (yr BP)	Calibrated age range[a] (95.4% probability) (cal yr BP)	Tau boundary[b] $\pm 1\sigma$ (cal yr BP)
Above Rotoehu Ash							
Pouto 2/3	Pouto 2[c]	Wk-8793	α-cellulose	22.9	41,430 ± 394	44,366–45,633	44,795 ± 316
Pouto 2/3	Pouto 2[c]	ANU-17604[d]	ABOX-SC:920	–	41,490 ± 740	44,035–46,232	
Pouto 2/3	Pouto 2[c]	UCI-16110/16111[e]	ABA	–	41,160 ± 315 (n=2)	44,279–45,376	
Pouto 2/4	Pouto 2[c]	Wk-8794	α-cellulose	18.5	41,056 ± 384	44,169–45,392	
Pouto 2/4	Pouto 2[c]	ANU-17606[d]	ABOX-SC:920	–	42,070 ± 890	44,163–47,386	
Pouto 2/4	Pouto 2[c]	UCI-16112/16113[e]	ABA	–	41,244 ± 315 (n=2)	44,325–45,430	
ARA*	Pouto 1[f]	ANU-13018[d]	ABA-SC:920	–	19,460 ± 330	22,345–23,977	-
ARA*	Pouto 1[f]	ANU-13019[d]	ABA-SC:650	–	19,070 ± 210	22,252–23,361	
ARA*	Pouto 1[f]	ANU-13016[d]	AOX-SC:920	–	19,030 ± 200	22,232–23,330	
ARA*	Pouto 1[f]	ANU-13017[d]	AOX-SC:650	–	18,970 ± 200	22,173–23,311	
Below Rotoehu Ash							
4BRA*	Pouto 1[f]	ANU-14103[d]	ABA-SC:910	–	42,930 ± 740	44,875–48,051	47,535 ± 2086
4BRA*	Pouto 1[f]	ANU-14104[d]	ABA-SC:650	–	42,840 ± 720	44,822–47,825	
4BRA*	Pouto 1[f]	ANU-15518[d]	ABOX-SC:910	–	43,800 ± 840	45,481–49,216	
BRA*	Pouto 1[f]	ANU-14105[d]	ABA-SC:910	–	47,690 ± 950	45,924–49,849	–
BRA*	Pouto 1[f]	ANU-14106[d]	ABA-SC:650	–	47,530 ± 940	45,780–49,663	
BRA*	Pouto 1[f]	ANU-13013[d]	AOX-SC:920	–	45,330 ± 1,410	46,302–…[g]	
BRA*	Pouto 1[f]	ANU-13014[d]	AOX-SC:650	–	46,820 ± 1,140	44,737–49,525	
BRA*	Pouto 1[f]	ANU-13502[d]	ABOX-SC:910	–	50,520 ± 1,240	48,272–53,534	
BRA*	Pouto 1[f]	ANU-13504[d]	ABOX-SC:650	–	45,700 ± 950	46,928–…[g]	
BRA*	Pouto 1[f]	ANU-15516[d]	CE-SC:910	–	49,820 ± 1,210	47,621–52,740	
Pouto 2/1	Pouto 2[c]	Wk-8791	α-cellulose	22.9	45,973 ± 649	47,602–…[g]	-
Pouto 2/1	Pouto 2[c]	ANU-16327[d]	ABOX-SC:920	–	47,970 ± 1,100	45,954–50,555	
Pouto 2/1	Pouto 2[c]	UCI-16105/16106[e]	ABA	–	44,625 ± 474 (n=2)	46,384–49,254	
Pouto 2/2	Pouto 2[c]	Wk-8792	α-cellulose	24.3	46,223 ± 673	47,832–…[g]	
Pouto 2/2	Pouto 2[c]	ANU-16504[d]	ABOX-SC:920	–	47,200 ± 970	45,400–49,415	
Pouto 2/2	Pouto 2[c]	UCI-16108/16109[e]	ABA	–	45,670 ± 534 (n=2)	47,481 - …[g]	

* Data from Santos et al. (2001).
[a] Southern Hermipshere dates minus 41 yr to account for SH offset (McCormac et al. 2002).
[b] Tau Boundary function of Oxcal 4.1.7 (Bronk Ramsey, 2010) as applied to the 2 most applicable datasets - see text for details.
[c] Pouto 2 location: 36°23′32.4″S 174°07′41.0″E.
[d] ANU dates calculated using estimated δ^{13}C value of −25‰.
[e] UCI results have been corrected for isotopic fractionation but δ^{13}C data not given here.
[f] Pouto 1 location: 36°23'29.2″S 174°07'29.0″E.
[g] Dates beyond the IntCal09 curve (> 50,000 cal yr BP).

conductive layer of gold and analysed using the UCLA CAMECA ims 1270 ion probe (SIMS). In order to investigate zircon growth patterns and detect possible zoning, ^{238}U/^{230}Th analysis was performed by continuous depth profiling perpendicular to growth layers using a 60 nA $^{16}O^-$ beam focused into a ~25 × 30 μm oval spot. Secondary ion intensities were recorded in 60 magnet cycles, corresponding to ~9 μm depth. To compensate for low abundance ions such as $^{230}Th^{16}O^+$ and gain a meaningful depth resolution, 30 cycles were integrated to produce two sets of rim ages from ~0–4.5 μm and from ~4.5–9 μm.

^{238}U/^{230}Th isotope analyses in zircon were performed following the protocols described in Schmitt et al. (2006, 2011). Electron-multiplier and Faraday cup detectors gains were calibrated by analysis of $^{235}UO^+$ and $^{238}UO^+$ and normalizing the background corrected ion intensities to $^{238}U/^{235}U = 137.88$ (Rosman and Taylor, 1998). U/Th relative sensitivities were calibrated from analyses of zircon standard 91500 with 81.2 ppm U and 28.61 ppm Th (Wiedenbeck et al., 1995). We verified the accuracy of the relative sensitivity calibration and background corrections on AS3 secular equilibrium standard (1099 Ma; Paces and Miller, 1993), which was mounted adjacent to the unknowns. The ^{230}Th/^{238}U weighted averages of AS3 analyses interspersed with the unknowns is 1.005 ± 0.009 (MSWD = 0.6; $n = 10$), consistent with secular equilibrium of AS3.

Zircon ^{238}U/^{230}Th ages were calculated as two-point isochrons through each of the zircon analyses and a model melt represented by the average of two published whole rock compositions from Rotoiti with (^{230}Th/^{232}Th) = 0.730 ± 0.003 and (^{238}U/^{232}Th) = 0.735 ± 0.002 (Charlier et al., 2003).

2.3. (U–Th)/He dating

Three sub-sets of zircons were dated by the (U–Th)/He method. First, given the young eruption age of the samples and expected low amount of ^{4}He in the crystals, 4–6 zircon crystals of similar size, shape and alpha retention factor (Ft; Farley et al., 1996) were selected and dated as multi-grain aliquots to increase the ^{4}He signal and detect potential analytical limitations. After proving the ^{4}He was detectable, individual zircon crystals were analysed. Finally, to perform double-dating, zircon crystals previously analysed by SIMS were plucked out from the mounts, cleaned of gold coating and processed for (U–Th)/He analysis as outlined below.

(U–Th)/He analysis followed the protocols described in Evans et al. (2005) and Schmitt et al. (2011). The crystals were transferred into niobium (Nb) tubes. (U–Th)/He dating was performed with ^{4}He, ^{238}U and ^{232}Th measured by quadrupole isotope-dilution mass spectrometry (MS) (for He) and inductively coupled plasma (ICP) MS (for U and Th). ^{4}He was extracted from zircon at ~1250 °C under high vacuum using a Nd-YAG laser, purified and analysed on the CSIRO Earth Science and Resource Engineering (John de Laeter Centre, Curtin University) extraction line Pfeiffer Prisma QMS-200 mass spectrometer. A "re-extract" was run after each sample to verify complete

outgassing of the crystals. Helium gas results were corrected for blank, determined by heating empty Nb tubes using the same procedure. Reproducibility of ^{4}He gas standards during this study was better than ~0.008% and ~0.1% (both 1σ) on a daily and long-term basis, respectively. After the ^{4}He measurements, Nb tubes containing the crystals were retrieved from the laser cell, loaded into Parrish vials, spiked with ^{235}U and ^{230}Th and dissolved in Parr bombs using HF and HCl. Sample, blank, and spiked standard solutions were analysed for ^{238}U and ^{232}Th at TSW Analytical Ltd (University of Western Australia) on an Agilent 7500 ICP MS (Evans et al., 2005). Total analytical uncertainty (TAU) was computed as the square root of the sum of the squares of weighted uncertainties on U, Th and He measurements. The TAU was used to calculate the uncertainty of raw (U–Th)/He ages.

The raw (U–Th)/He ages were corrected for alpha ejection after Farley et al. (1996) assuming a homogeneous distribution of U and Th. Since the error of the Ft correction increases with decreasing crystal size (Farley et al., 1996), values of 5% and 10% were adopted as the Ft correction uncertainties for large ($Ft \geq 0.6$) and small crystals ($Ft < 0.6$), respectively.

(U–Th)/He zircon ages calculated assuming U-series equilibrium will significantly underestimate young eruption ages because deficits in the long-lived intermediate daughter isotope ^{230}Th (half-life ~75.69 ka) are common. ^{231}Pa excess (half-life ~32.76 ka), by contrast, produces He that is unsupported if radioactive equilibrium at the time of crystallization is assumed (Farley et al., 2002). U-series radioactive decay during pre-eruptive crystal residence reduces the degree of disequilibrium (Farley et al., 2002). To correct zircon (U–Th)/He ages for disequilibrium and pre-eruptive crystal residence, we used the MCHeCalc software (Schmitt et al., 2010) that requires as input parameters the Ft-corrected zircon (U–Th)/He ages and uncertainties, the zircon crystallization ages and uncertainties, and so-called D_{230} and D_{231} parameters describing zircon-melt fractionation of Th and Pa relative to U (Farley et al. 2002; Schmitt et al., 2010).

For the purpose of illustrating the effect of disequilibrium and pre-eruptive crystal residence, we first corrected (U–Th)/He ages for secular disequilibrium in zircon-producing magma by adopting a value of 0.2 for the D_{230} parameter (Charlier and Zellmer, 2000; Farley et al., 2002). This approach neglects pre-eruptive crystal storage during which the deficit in ^{230}Th diminishes. It thus maximises the disequilibrium correction of (U–Th)/He ages, providing an upper (older) limit for the eruption age. This over-simplified correction can be refined by taking into account constraints from SIMS ^{238}U/^{230}Th analysis which permits calculating D_{230} by dividing measured Th/U ratios of zircons by published whole-rock Th/U ratios of 4.1870 (EQF) and 4.1257 (Rotoiti), determined by TIMS (Charlier et al., 2003). For constraining D_{230}, we also assumed that the magma was in secular equilibrium and that the measured whole-rock values are representative for the magma from which the zircons originated, a reasonable assumption given the limited variation in Th/U and the near-secular equilibrium composition of OVC rhyolites (Charlier et al., 2003; Charlier and Wilson, 2010). The main advantage of double-dating is that ^{238}U/^{230}Th ages constrain the duration of pre-eruptive residence. Thus, where available, we used the ^{238}U/^{230}Th model rim crystallization ages and their associated uncertainties to estimate pre-eruptive residence. For crystals that have not been analysed by SIMS ^{238}U/^{230}Th, we used error weighted average and standard deviation of all 'rim' ^{238}U/^{230}Th analyses as representative of the zircon crystallization age and uncertainty (Table 1). For D_{231} (a minor correction because of the low abundance of ^{235}U) we adopted the published Pa/U zircon-rhyolite melt partitioning ratio of 3 (Schmitt, 2007), resulting in a slight decrease of the (U–Th)/He ages.

Average (U–Th)/He ages ($n=22$ for EQF and $n=20$ for Rotoiti sample) are reported as best-fit eruption ages stating uncertainties at the 95% confidence level (2σ) which were calculated by multiplying the 2-sigma errors by the square root of the MSWD and Student's-t for N-1 degrees of freedom using the Isoplot add-in for Excel (Ludwig, 2003). To enable direct comparison with ^{14}C calendar dates, eruption ages are reported in calendar years before present (BP) where present = 1950 AD.

2.4. ^{14}C dating

Two wood samples from both above and below the Rotoehu tephra were analysed by three laboratories (Table 1). Those analysed by high precision liquid scintillation (LS) spectroscopy at the University of Waikato ('Wk' in Table 1) were pre-treated to α-cellulose, converted to benzene, and analysed by Perkin Elmer Quantulus spectrometers based on the protocols described in Hogg et al. (2007). All results were corrected for δ^{13}C, with background blank correction (equivalent to an apparent age of 58.2 ka BP) achieved by ^{14}C analysis of the α-cellulose fraction of Marine Isotope Stage (MIS) 7 (~170 ka) wood (Hogg et al., 2006). Duplicates were analysed by accelerator mass spectrometry (AMS) at the Australian National University ('ANU' in Table 1) and at the Keck Carbon Cycle AMS laboratory at the University of California at Irvine ("UCI" in Table 1). The ANU analyses utilized acid–base-wet oxidation pretreatment with stepped combustion (ABOX-SC) and a combustion temperature of 910 °C. The δ^{13}C values were estimated as −25‰. Background blank correction (equivalent to an apparent age of 54.7 ka BP) was achieved by ^{14}C analysis of MIS 5 (~120 ka) wood (Santos et al., 2001). The UCI analyses utilised acid–base–acid (ABA) wash pretreatment at ~70 °C with 1 N HCl and 1 N NaOH, with the base washes repeated until the extract humic acid was fully removed. All results were corrected using the on-line δ^{13}C AMS values of the respective graphite aliquots measured, following instrumental analysis described in Santos et al. (2007). The blank correction was obtained from ^{14}C analysis of the same set of MIS 5 wood samples as those used in the ANU measurements, subjected to the standard ABA pretreatment mentioned above.

The resulting ages are reported both as conventional ^{14}C ages (yr BP) as well as 95.4% (2-sigma) probability calendar age ranges (cal yr BP) calibrated by OxCal 4.1 (Bronk Ramsey, 2009) using the IntCal09 calibration curve (Reimer et al., 2009).

Santos et al. (2001) previously reported uncalibrated AMS ^{14}C ages on wood samples from the site Pouto 1, 300 m west of the Pouto site (Pouto site 2) examined here (Table 1). The ages from above the tephra (ARA sample) are young (~23 ka cal BP) and thus provide little constraint on the age of the eruption. These ages suggest a lag time of ~20 kyr between the deposition of the tephra and growth of the trees at this site and hiatuses in sediment deposition. Santos et al. (2001) also presented 10 age estimates on two wood samples from beneath the tephra layer. Three of them (4BRA sample) are stratigraphically constrained to 4 cm below the tephra layer, while the remainder (BRA sample) occurred at unspecified positions below. We consider that the 4BRA sample ages are more relevant to this study and consider them in more detail below. For comparison with our new data, we have converted all the Santos et al. (2001) data to calendar ages (Table 1).

3. Results

3.1. ^{14}C ages

The new analyses on wood samples from below the tephra returned finite ^{14}C ages ranging from 44.6 ± 0.5 to 48.0 ± 1.1 ka BP. The three 4BRA results (Santos et al., 2001) (between 42.8 ± 0.7 and 43.8 ± 0.8 ka BP) are slightly younger than the

new ages reported here. Since there is good agreement between the Waikato and ANU duplicate measurements, despite the differences in pretreatment and analytic techniques, the younger 4BRA sample ages are also considered reliable. Because the 4BRA ages are younger than our new samples underlying the Rotoehu tephra, we consider the 4BRA ages to represent the best approximation for the maximum age of the eruption.

OxCal 4.1 (Bronk Ramsey, 2009) and the IntCal09 ^{14}C calibration curve (Reimer et al. 2009) were used to provide calibrated calendar age ranges (Table 1). Whilst the younger 4BRA samples provide finite maximum 95.4% probability calendar age ranges (44.8–49.2 ka cal BP), some of the probability distributions for our new results from below the tephra extend beyond the limit of IntCal09, returning maximum 95.4% probability calendar age ranges from 45.4 to >50 ka cal BP (Table 1).

Two samples (Pouto 2/3 and 2/4 in Table 1) directly overlying the Rotoehu tephra produced finite ^{14}C ages in the range from 41.1 ± 0.4 to 42.1 ± 0.9 ka BP ($n=6$). These correspond to a maximum 95.4% probability calendar age range of 44.0–47.4 ka cal BP using IntCal09, and provide a minimum age range for the Rotoehu tephra. Given the IntCal09 calibration curve (Reimer et al., 2009) extends beyond the probability distribution for these ^{14}C ages, we consider this mean age to be more accurate and precise than the ages of samples underlying the tephra.

A Bayesian calibration model incorporating stratigraphic information as well as age data was developed within OxCal 4.1.7 (Bronk Ramsey, 2010). The wood samples most closely defining the age of the eruption (the 4BRA Pouto 1 samples beneath and the Pouto 2 samples above), were divided stratigraphically into two phases, according to whether they are pre-eruption, or post-eruption (Fig. 1A

Table 2
^{238}U/^{230}Th disequilibrium analytical results.

Sample	Analysis	(^{238}U/^{232}Th)	±1σ	(^{230}Th/^{232}Th)	±1σ	Age (ka)	+1σ	−1σ
Earthquake Flat								
EQ1-r	Outer rim	3.85	0.06	2.02	0.09	56.9	5.4	−5.2
EQ1-i	Inner rim	4.22	0.07	2.70	0.11	89.5	8.7	−8.1
EQ2-r	Outer rim	4.84	0.13	2.95	0.20	83.4	13.0	−11.6
EQ2-i	Inner rim	4.97	0.07	4.41	0.20	217.2	49.6	−34.0
EQ3-r	Outer rim	6.45	0.15	3.08	0.18	57.1	6.3	−5.9
EQ3-i	Inner rim	7.29	0.11	4.29	0.22	84.9	8.7	−8.0
EQ4-r	Outer rim	3.89	0.11	2.19	0.11	66.2	8.0	−7.4
EQ4-i	Inner rim	3.63	0.05	2.17	0.09	73.7	7.5	−7.1
EQ5-r	Outer rim	4.02	0.09	2.29	0.10	68.7	6.8	−6.4
EQ5-i	Inner rim	4.17	0.08	2.79	0.10	98.5	9.3	−8.6
EQ6-r	Outer rim	4.05	0.07	2.35	0.10	71.4	6.7	−6.3
EQ6-i	Inner rim	5.28	0.08	3.26	0.14	87.7	8.1	−7.5
EQ7-r	Outer rim	3.51	0.06	2.38	0.08	96.2	8.8	−8.1
EQ7-i	Inner rim	3.84	0.05	2.46	0.10	86.9	8.5	−7.9
EQ8-r	Outer rim	4.12	0.05	2.55	0.11	82.5	8.2	−7.6
EQ8-i	Inner rim	3.91	0.05	2.46	0.09	83.9	7.5	−7.0
EQ9-r	Outer rim	4.44	0.10	2.32	0.12	60.0	6.9	−6.5
EQ9-i	Inner rim	4.13	0.09	2.55	0.11	82.4	8.4	−7.8
EQ10-r	Outer rim	4.48	0.06	2.66	0.12	78.0	7.7	−7.2
EQ10-i	Inner rim	4.32	0.05	2.36	0.10	64.9	5.7	−5.4
EQ11-r	Outer rim	4.31	0.07	2.65	0.13	82.7	9.2	−8.5
EQ11-i	Inner rim	5.11	0.09	3.28	0.18	93.9	11.4	−10.3
EQ12-r	Outer rim	3.23	0.05	1.95	0.06	71.8	5.3	−5.1
EQ12-i	Inner rim	3.80	0.05	2.36	0.09	81.2	7.1	−6.7
Weighted average of 'outer rim' ages (ka) ± Std. dev. (ka) (MSWD)						**69.7 ± 12.1 (3.0)**		
Weighted average of 'inner rim' ages (ka) ± Std. dev. (ka) (MSWD)						**85.7 ± 39.3 (1.5)**		
Rotoiti								
R1-r	Outer rim	3.69	0.05	1.86	0.13	52.9	8.2	−7.6
R1-i	Inner rim	3.80	0.05	1.90	0.14	52.2	8.7	−8.0
R2-r	Outer rim	5.87	0.12	3.22	0.26	72.7	11.8	−10.7
R2-i	Inner rim	5.07	0.10	2.18	0.21	44.5	8.5	−7.9
R3-r	Outer rim	4.36	0.12	1.88	0.23	41.5	10.6	−9.7
R3-i	Inner rim	4.31	0.12	2.42	0.26	70.1	16.3	−14.2
R7-r	Outer rim	5.28	0.13	2.51	0.24	54.3	10.2	−9.3
R7-i	Inner rim	4.25	0.07	2.27	0.19	63.2	11.0	−10.0
R9-r	Outer rim	4.85	0.12	2.65	0.25	68.5	13.5	−12.0
R9-i	Inner rim	4.27	0.08	1.97	0.18	47.0	8.9	−8.2
R11-r	Outer rim	5.35	0.11	2.80	0.22	64.9	10.0	−9.2
R11-i	Inner rim	4.78	0.08	3.00	0.18	89.8	12.2	−11.0
R12-r	Outer rim	3.49	0.05	1.78	0.13	52.6	9.1	−8.4
R12-i	Inner rim	3.51	0.06	1.66	0.13	44.3	8.0	−7.5
R13-r	Outer rim	3.64	0.05	1.73	0.12	46.2	7.5	−7.0
R13-i	Inner rim	3.61	0.06	1.65	0.13	42.4	7.8	−7.2
R14-r	Outer rim	5.60	0.16	2.87	0.20	63.4	8.8	−8.2
R14-i	Inner rim	6.48	0.11	2.65	0.29	44.6	8.8	−8.2
R15-r	Outer rim	6.08	0.14	2.63	0.33	48.1	11.0	−10.0
R15-i	Inner rim	5.58	0.15	2.78	0.26	60.2	11.1	−10.1
R5R-r	Outer rim	5.50	0.16	2.65	0.32	56.4	13.4	−11.9
R5R-i	Inner rim	4.98	0.10	2.30	0.24	50.5	10.3	−9.4
R10R-r	Outer rim	6.22	0.16	3.08	0.33	61.2	12.4	−11.2
R10R-i	Inner rim	6.23	0.16	3.32	0.32	69.5	13.2	−11.7
Weighted average of 'outer rim' ages (ka) ± Std. dev. (ka) (MSWD)						**55.6 ± 9.4 (1.0)**		
Weighted average of 'inner rim' ages (ka) ± Std. dev. (ka) (MSWD)						**51.0 ± 14.5 (2.0)**		

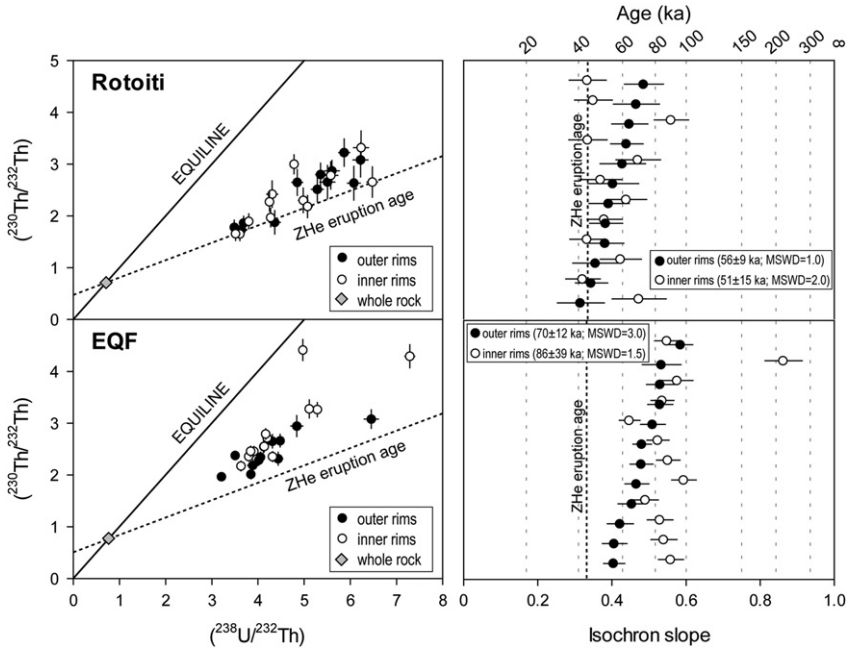

Fig. 3. Left - zircon model-age data for the Rotoiti and EQF tephras. The $^{230}Th/^{232}Th$ vs $^{238}U/^{232}Th$ equiline and isochrons for the eruption ages determined from ZHe data are shown for reference. Error bars represent 1σ analytical uncertainties. Right - rank order plots for the Rotoiti and EQF tephras showing distribution of zircon $^{238}U/^{232}Th$ model ages based on isochron slopes. The plots are ranked according to the 'outer rim' ages; associated 'inner rim' ages and eruption ages are shown for comparison. Error bars represent 1 sigma analytical uncertainties.

in Supplementary files). We then generated modeled maximum probability ages for the eruption group boundaries using the "Tau_-Boundary" function (pre-eruption boundary 47.5 ± 2.1 ka cal BP; post-eruption boundary 44.8 ± 0.3 ka cal BP; Table 1). We consider the error term for the Pouto 2 upper Tau boundary as shown in Table 1 is probably an under-estimation, because of the paucity of datapoints in IntCal09 in the 40–50 ka BP age range.

3.2. Zircon $^{238}U/^{230}Th$+(U–Th)/He ages

Twelve crystals from Rotoiti pumice produced crystallization ages in the range 42.4+7.8/−7.2 to 89.8+12.2/−11.0 ka (inner rims) and 41.5+10.6/−9.7 to 72.7+11.8/−10.7 ka (outer rims) (Table 2; Fig. 3). Twelve crystals from EQF pumice produced ages in the range 64.9+5.7/−5.4 to 217.2+49.6/−34.0 ka (inner rims) and 56.9+5.4/−5.2 to 96.2+8.8/−8.1 ka (outer rims). In most cases, the inner and outer rim ages overlap at the 2σ level. The exceptions are five EQF crystals in which the inner rims are up to ~130 ka older than the outer rims. The overall zircon crystallization age range, and the somewhat older age population in EQF relative to Rotoiti agrees with published spot analyses of the interiors of sectioned crystals using SHRIMP-RG instrumentation: 50 ± 25 to 236 ± 126 ka (Rotoiti) and 70 ± 30 to 226 ± 118 ka (EQF; Charlier et al., 2003; Charlier and Wilson, 2010). Charlier et al. (2003) also report multi-grain bulk crystal separate TIMS results (comprising an estimated ~100–200 zircon crystals) which yielded isochron ages of ~70 ka and ~173 ka for Rotoiti and EQF, respectively. These bulk crystal separate ages broadly agree with the averages from individual spot analyses.

(U–Th)/He results are summarized in Table 3 and Fig. 4. Averaging individual Ft corrected ages, a relatively high scatter, indicated by elevated mean square of weighted deviates (MSWD) of 3.6 and 2.0, respectively, is interpreted as resulting from our simplified assumptions regarding zircon crystal geometry, the distribution of parent nuclides, the presence of undetected inclusions, and other imperfections of the crystals affecting the accuracy of the Ft correction. Prior to correction for disequilibrium, (U–Th)/He ages of individual aliquots are also all younger than corresponding $^{238}U/^{230}Th$ ages which date magmatic crystallization. This provides a first-order consistency check of the method, and we will further discuss the relationships between disequilibrium-corrected (U–Th)/He and $^{238}U/^{230}Th$ ages below.

Results of statistical tests for homogeneity and outliers (e.g., Grubbs, Dixon's Q, chi-square, Anova, G-test) showed that there is no statistically significant difference in (U–Th)/He ages measured on multi-grain and single-grain aliquots, or by double- and non-double-dating analytical approaches. Thus, all replicates of individual samples were treated as one population when calculating an average eruption age. Neglecting for now pre-eruptive zircon residence time, we calculate average disequilibrium corrected (U–Th)/He ages for D_{230} of 0.2 (Charlier and Zellmer, 2000; Farley et al., 2002) of 49.2 ± 3.7 ka (2σ; n=20; MSWD=3.9) for Rotoiti zircons and 52.7 ± 3.2 ka (2σ; n=22; MSWD=2.9) for EQF (Table A2 in Supplementary files). We emphasize that these ages strictly define a maximum estimate for the eruption because pre-eruptive zircon residence will mitigate the effect of disequilibrium. These ages also display excess scatter as indicated by elevated MSWDs. Because pre-eruptive crystal residence will reduce the extent of the ^{230}Th disequilibrium, these (U–Th)/He maximum ages in fact significantly overestimate the true eruption age.

To resolve this overcorrection, we consider pre-eruptive residence which lessens the initial disequilibrium inferred from zircon and melt partitioning behaviour (the D_{230} parameter). We and others (Charlier et al. 2003, 2010) have determined zircon crystallization model ages that are on average 10's of thousands of years older than existing eruption age estimates for Rotoiti and EQF. Consequently, the residence-time corrected (U–Th)/He ages for the Rotoiti and EQF zircons using $^{238}U/^{230}Th$ model ages (see above), shift to younger ages (45.1(7)[1] ± 3.3 ka; 2σ; n=20; MSWD=3.6, and 45.1(6)[1] ± 2.9 ka; 2σ; n=22; MSWD=2, respectively, Table 3; second decimal only shown for distinction of

[1] Second decimal only shown for distinction of values.

Table 3
(U–Th)/He analytical results and parameters used for the disequilibrium correction [a].

Sample code	N_c	Dating method	^{232}Th (ng)	± (%)	^{238}U (ng)	± (%)	^{4}He (ncc)	± (%)	TAU (%)	Unc. age (ka)	± 1σ (ka)	F_t	F_t-Cor. age (ka)	± 1σ (ka)	^{238}U/^{230}Th age (ka)	± 1σ (ka)	D_{230}	Dsq.-Cor. age (ka)	± 1σ (ka)
Earthquake Flat																			
EQF-M-1	5	He	2.931	3.8	2.637	4.1	0.0089	2.3	4.0	21.9	0.9	0.65	33.9	3.7	69.7[b]	12.1	0.264	48.0	5.5
EQF-M-2	5	He	1.577	3.8	2.007	2.8	0.0061	3.1	4.0	20.9	0.8	0.65	32.0	3.4	69.7[b]	12.1	0.186	48.2	5.8
EQF-M-3	5	He	1.048	1.7	1.518	2.0	0.0032	3.4	3.8	14.8	0.6	0.59	25.3	2.7	69.7[b]	12.1	0.164	37.4	4.8
EQF-M-4	5	He	0.403	3.7	0.584	2.7	0.0020	5.4	5.9	24.8	1.5	0.69	35.8	2.8	69.7[b]	12.1	0.164	54.5	5.3
EQF-S-1	1	He	2.675	3.9	1.546	4.2	0.0058	5.4	6.3	21.9	1.4	0.65	34.0	2.7	69.7[b]	12.1	0.410	42.5	3.7
EQF-S-2	1	He	0.881	3.9	1.042	4.1	0.0040	11.9	12.4	26.6	3.3	0.74	36.1	4.8	69.7[b]	12.1	0.200	53.5	7.6
EQF-S-3	1	He	0.342	3.8	0.449	2.8	0.0013	23.9	24.0	19.9	4.8	0.72	27.8	6.8	69.7[b]	12.1	0.181	40.4	10.8
EQF-S-4	1	He	0.596	3.8	0.900	4.1	0.0031	3.6	5.1	24.3	1.2	0.69	35.2	2.5	69.7[b]	12.1	0.157	54.0	5.0
EQF-S-5	1	He	0.797	3.8	1.009	4.1	0.0029	2.2	4.2	19.9	0.8	0.71	27.9	1.8	69.7[b]	12.1	0.187	41.4	3.5
EQF-S-6	1	He	1.102	3.8	1.192	4.1	0.0041	3.2	4.7	23.5	1.1	0.68	34.3	2.4	69.7[b]	12.1	0.219	49.1	4.3
EQF-S-7	1	He	0.705	3.7	1.042	3.7	0.0027	7.2	7.9	18.4	1.5	0.76	24.2	2.3	69.7[b]	12.1	0.160	36.0	4.3
EQF-S-8	1	He	0.394	3.7	0.662	2.8	0.0021	8.9	9.2	22.7	2.1	0.71	31.9	3.4	69.7[b]	12.1	0.141	49.8	6.2
EQF-S-9	1	He	0.707	3.7	0.762	2.8	0.0019	1.8	3.0	16.7	0.5	0.52	32.2	3.4	69.7[b]	12.1	0.220	45.6	5.7
EQ-2	1	SIMS+He	0.468	3.7	0.693	3.3	0.0020	6.4	7.0	20.9	1.5	0.61	34.4	3.0	83.4	13.0	0.160	49.2	5.4
EQ-3	1	SIMS+He	0.760	3.7	1.011	3.2	0.0025	7.5	8.0	17.2	1.4	0.66	26.1	2.5	57.1	6.3	0.178	40.7	4.5
EQ-4	1	SIMS+He	1.544	3.7	1.786	3.2	0.0049	2.7	3.8	18.9	0.7	0.72	26.3	1.7	66.2	8.0	0.205	38.2	3.0
EQ-5	1	SIMS+He	0.730	3.7	1.136	3.2	0.0036	3.1	4.2	22.8	1.0	0.67	34.2	2.2	68.7	6.8	0.152	53.5	4.4
EQ-7	1	SIMS+He	0.404	3.7	0.545	2.8	0.0016	4.2	4.9	20.4	1.0	0.63	32.5	2.3	96.2	8.8	0.176	43.7	3.6
EQ-8	1	SIMS+He	0.740	3.7	0.846	2.9	0.0028	6.4	6.9	22.4	1.5	0.69	32.5	2.8	82.5	8.2	0.207	44.9	4.3
EQ-9	1	SIMS+He	0.773	3.7	0.950	3.3	0.0025	2.1	3.6	18.5	0.7	0.68	27.2	1.7	60.0	6.9	0.193	41.7	3.2
EQ-10	1	SIMS+He	0.915	3.7	1.121	2.9	0.0046	3.5	4.3	28.2	1.2	0.70	40.4	2.7	78.0	7.7	0.194	58.7	4.9
EQ-11	1	SIMS+He	2.732	3.7	1.862	4.2	0.0078	2.3	4.0	25.7	1.0	0.55	47.0	5.1	82.7	9.2	0.348	60.3	7.0
Best-fit eruption age (ka) ± 2σ (ka) (MSWD)																		**45.16 ± 2.90 (2.0)**	
Rotoiti																			
ROT-M-1	5	He	1.758	3.8	1.931	4.1	0.0065	1.9	4.0	22.7	0.9	0.68	33.5	3.6	55.6[b]	9.4	0.219	50.2	5.6
ROT-M-2	5	He	1.859	3.8	1.978	2.9	0.0070	1.6	2.9	23.7	0.7	0.66	35.8	3.7	55.6[b]	9.4	0.226	54.4	5.5
ROT-S-1	1	He	0.409	3.8	0.361	2.8	0.0014	4.6	5.2	25.9	1.3	0.70	36.8	2.6	55.6[b]	9.4	0.273	52.9	3.9
ROT-S-2	1	He	0.422	3.9	0.484	4.1	0.0019	7.6	8.3	26.2	2.2	0.80	32.8	3.2	55.6[b]	9.4	0.210	50.7	5.1
ROT-S-3	1	He	0.996	5.4	1.105	5.7	0.0042	1.2	4.9	25.6	1.3	0.77	33.2	2.3	55.6[b]	9.4	0.217	50.5	3.8
ROT-S-4	1	He	1.362	3.8	1.244	4.2	0.0044	1.3	3.6	23.0	0.8	0.80	28.8	1.8	55.6[b]	9.4	0.263	41.5	3.0
ROT-S-5	1	He	0.822	3.8	1.101	4.1	0.0033	4.4	5.7	21.1	1.2	0.77	27.3	2.1	55.6[b]	9.4	0.180	43.1	3.9
ROT-S-6	1	He	0.160	3.8	0.265	2.9	0.0007	6.7	7.1	19.7	1.4	0.65	30.4	2.7	55.6[b]	9.4	0.146	49.8	4.8
ROT-S-7	1	He	0.301	3.7	0.381	2.9	0.0014	10.0	10.4	25.1	2.6	0.61	41.4	4.8	55.6[b]	9.4	0.190	63.9	6.7
R-1	1	SIMS+He	0.682	3.7	0.823	3.6	0.0018	2.7	4.1	15.2	0.6	0.73	20.9	1.4	52.9	8.2	0.199	32.1	2.6
R-2	1	SIMS+He	0.534	3.7	0.635	3.0	0.0017	6.7	7.2	18.4	1.3	0.67	27.5	2.4	72.7	11.8	0.202	39.1	3.9
R-3	1	SIMS+He	1.400	3.7	1.845	3.0	0.0054	3.8	4.6	20.3	0.9	0.79	25.9	1.8	41.5	10.6	0.183	42.4	3.2
R-5	1	SIMS+He	0.398	3.7	0.466	3.3	0.0015	2.0	3.4	21.8	0.7	0.71	30.7	1.9	56.4	13.4	0.206	46.1	3.6
R-7	1	SIMS+He	0.670	3.7	0.810	2.8	0.0020	2.1	3.2	16.6	0.5	0.62	26.9	1.6	54.3	10.2	0.199	41.5	3.1
R-9	1	SIMS+He	0.386	3.7	0.498	2.8	0.0014	5.8	6.3	19.2	1.2	0.69	28.0	2.3	68.5	13.5	0.187	40.7	4.3
R-11	1	SIMS+He	0.665	3.7	0.812	2.8	0.0027	4.1	4.8	23.0	1.1	0.73	31.3	2.2	64.9	10.0	0.197	46.9	4.0
R-12	1	SIMS+He	1.189	3.7	1.176	3.1	0.0044	3.7	4.5	25.1	1.1	0.72	35.0	2.4	52.6	9.1	0.243	51.9	3.7
R-13	1	SIMS+He	0.814	3.7	0.816	3.0	0.0029	1.8	3.1	23.7	0.7	0.65	36.3	2.1	55.6[c]	9.4	0.240	54.1	3.3
R-14	1	SIMS+He	1.147	3.7	1.105	3.1	0.0035	2.9	3.8	20.7	0.8	0.74	27.9	1.8	63.4	8.8	0.250	39.9	3.1
R-15	1	SIMS+He	0.365	3.7	0.473	2.9	0.0015	1.3	2.8	21.5	0.6	0.67	32.1	1.8	48.1	11.0	0.186	50.7	3.1
Best-fit eruption age (ka) ± 2σ (ka) (MSWD)																		**45.17 ± 3.30 (3.6)**	

[a] N_c - number of dated zircon crystals; Dating method: He - conventional (U–Th)/He dating; SIMS+He - the crystal double-dated by ^{238}U/^{230}Th and (U–Th)/He methods; ^{4}He - volume of helium in ncc at STP; TAU - total analytical uncertainty; Unc. age - uncorrected (U–Th)/He age; F_t - alpha retention factor after Farley et al. (1996); F_t-Cor. age - (U–Th)/He age corrected for alpha ejection; ^{238}U/^{230}Th age - determined by SIMS in this study; D_{230} - Th zircon-melt fractionation factor (Farley et al. 2002); Dsq.-Cor. age - (U–Th)/He age corrected for disequilibrium.

[b] ^{238}U/^{230}Th age and uncertainty calculated as weighted average and standard deviation from all 'outer rim' ^{238}U/^{230}Th ages of double-dated crystals.

[c] Average ^{238}U/^{230}Th age and uncertainty used because the original SIMS age appeared to young and caused failure of the MCHeCalc software.

values) relative to the overestimated age resulting from disequilibrium-only correction.

The statistically insignificant age difference of 0.01 ka (P-value = 0.9834) between Rotoiti and EQF (U–Th)/He eruption ages is consistent with the brief hiatus between the two eruptions inferred from the field observations (Nairn and Kohn, 1973; Wilson et al., 2007). These ages also fall within the 44.8 ± 0.3 to 47.5 ± 2.1 ka cal BP time window permitted by stratigraphically bracketing ^{14}C ages (Fig. 4).

The residence-time correction also results in MSWD values for the best-fit averages that are slightly lower than the (U–Th)/He ages corrected only for disequilibrium. They are, however, still outside the 95% confidence interval for a homogenous population (Mahon, 1996). We deem it unlikely that rapid cooling during the eruption could have produced anything other than a homogeneous (U–Th)/He age population. Therefore, the elevated MSWD implies that propagated analytical uncertainties may not fully account for the actual analytical scatter. The (minor) unaccounted analytical uncertainty likely results from simplified model assumptions regarding the (U–Th)/He ages corrections: uniformity in U and Th abundances and crystallization ages for the individual crystals. If, for example, U and Th were enriched in crystal rims relative to the interiors, the Ft correction (assuming uniform abundances) would incompletely account for the actual loss of radiogenic ^{4}He, which would result in an underestimation of the true age (the opposite would be the case for U and Th depletions at the crystal margins). SIMS rim analyses that sequentially sample deeper parts of the crystal display little evidence for U and Th zonation, although two crystals are enriched in U within the outer rim by ~70% relative to the inner rim crystal domain. Considering age zonation, it can be reasonably assumed that rims crystallized subsequent to interior

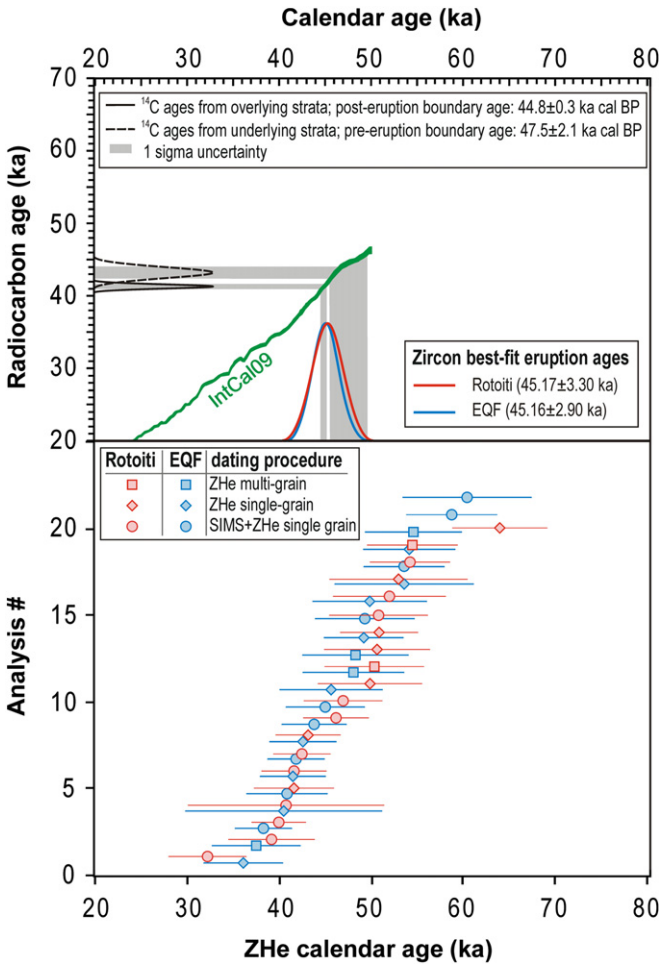

Fig. 4. Summary of the zircon (U–Th)/He (ZHe) and ^{14}C dating results. Upper panel: brackets (grey strips) for the eruptions, defined by the modelled ^{14}C Tau boundaries in calendar years (horizontal axis at top) using the IntCal09 calibration curve (Reimer et al., 2009), are projected on the best-fit eruption ages from zircon double-dating (blue and red Gaussian curves). Lower panel: Ranked Ft- and disequilibrium-corrected zircon (U–Th)/He ages.

domains, and that symmetry allows for extrapolating ages analysed at one rim to the entire crystal (cf. Storm et al. (2011) for occurrences of asymmetric age zonation). The simplifying assumption of a uniform crystallization age will either tend to underestimate the bulk crystallization age (in the case of using "rim" ages), or result in an over- or under-correction if the crystal is on average older or younger than the "average" crystallization age used. At present, we see no efficient solution to extract information on crystal compositional and age zonation for a more sophisticated correction of (U–Th)/He zircon ages. Instead, we deem it more practical to minimize bias resulting from simplified assumptions regarding composition and age heterogeneity by (1) replicate analysis of crystals from individual samples; (2) propagating crystallization age uncertainties over the sampled crystal population; and (3) multiplying the error of the weighted average by the square-root of the MSWD.

4. Discussion and implications

4.1. Comparison with previous age estimates for the Rotoiti eruption

The commonly cited age for Rotoehu tephra (61.0 ± 1.4 ka) (Wilson et al., 2007) was calculated as an average from obsidian K/Ar ages of 62 ± 12, 65 ± 16, and 63 ± 18 ka (2σ uncertainties; Wilson et al., 1992) from bracketing glassy lava flows; and an additional obsidian ^{40}Ar/^{39}Ar age of 58.5 ± 1.1 ka from an overlying lava on Mayor Island (Wilson et al., 2007). The latter is significant because it would provide a minimum age. This age is based on step-heated gas release that produces a distinct plateau and isochron with no evidence of age discordance. However, its accuracy is difficult to assess without knowledge of consistency with other lavas in the sequence that have not been dated by the ^{40}Ar/^{39}Ar method. In some situations, extraneous Ar and undetected microscopic xenocrystic or antecrystic materials in groundmass have shown to produce erroneously old ages (e.g., McDougall et al., 1969; Villa, 1991; Esser et al., 1997; Renne et al., 1997; Singer et al., 1998; Cassata et al., 2010). Glassy rocks are also known to be susceptible to weathering and hydration, which may affect argon retention and/or alkali exchange (Kaneoka, 1972; Walker and McDougall, 1982; Foland et al., 1993), and kinetic fractionation of Ar isotopes (Morgan et al., 2009). We suggest this lava flow and others in the sequence require further investigation.

^{14}C data pertaining to the Rotoiti/EQF eruptions have previously been subject to intense discussion (e.g., Froggatt and Lowe, 1990; Lowe and Hogg, 1995). It is commonly held that some ^{14}C ages are problematic because of poor preservation conditions at the sampling sites, incomplete removal of contamination during pretreatment of the samples, or inadequate blank corrections (e.g., Froggatt and Lowe, 1990; Lowe and Hogg, 1995). We restrict our discussion to comparing the new (U–Th)/He and ^{14}C data to estimates (both ^{14}C and other) that are yet to be disproven. The best-fit (U–Th)/He zircon ages are $45.1(7) \pm 3.3$ ka for the Rotoiti and $45.1(6) \pm 2.9$ ka for the EQF eruption, with upper limits of 50.1 ± 2.0 ka and 52.7 ± 3.2 ka (without residence time correction), respectively. These ages are consistent within uncertainties with the following independently determined ages (quoted in calendar years): (1) ^{14}C ages of >41 ka (Thompson, 1968), 44.2 ± 4.3 ka (Grant-Taylor and Rafter, 1971) and $\sim 47.5 \pm 2.1$ ka (Santos et al., 2001 and this study), (2) optical luminescence ages on underlying paleosols of 44 ± 3 and 44 ± 8 ka (Lian and Shane, 2000), (3) palynological, magnetostratigraphic and sedimentation based ages of $\sim$44.3 to 52 ka in lake sediments (Shane and Sandiford, 2003; Molloy et al., 2009; Nilsson et al., 2011), (4) the age of $\sim$45 ka from sedimentation rates in deep-sea cores (Shane et al., 2006), and (5) an age of $\sim$45 ka from deep-sea oxygen isotope stratigraphy (acknowledged as low resolution) (Allan et al., 2008). Wilson et al. (2007) reported ^{40}Ar/^{39}Ar ages on biotite in Rotoiti (47.0 ± 3.8 ka) and EQF (54.7 ± 5.3 ka) deposits that are in good agreement with the (U–Th)/He ages reported here. However, Wilson et al. (2007) also reported additional determinations of >60 ka on biotites, and suggested the high atmospheric argon contents may affect the results (see also Hora et al., 2011 for problems with excess Ar in biotite).

^{238}U/^{230}Th disequilibrium zircon ages reflect crystallisation in the magma system, and individual crystals can record protracted (in some cases by 100's of ka) crystallization or residence prior to eruption (e.g., Schmitt, 2011). However, the youngest crystallisation age(s) define an upper limit for the eruption age. The 71 Rotoiti crystal interior ages reported in Charlier and Wilson (2010) display a peak in the probability density function curve at 60.4 ka, but the distribution includes crystal analyses younger (outside uncertainties) than their preferred eruption age of 61 ka, including $40+/-6$ ka, and $40+9/-8$ ka (see Fig. 4 in Charlier and Wilson, 2010). Charlier et al. (2003) reported a youngest age of $46+5/-4$ ka for a zircon from a plutonic clast within the Rotoiti ignimbrite. An explanation for such young ages, given their preferred eruption age of 61 ka, is not obvious, and non-constrained errors in the ^{230}Th/^{232}Th ratio were suggested

(Charlier and Wilson, 2010). $^{238}U/^{230}Th$ disequilibrium data for Rotoiti zircons determined here also include ages significantly less than 61 ka (Fig. 3), such as $41.5+10.6/-9.7$ ka, $42.4+7.8/-7.2$ and others (see Table 2). Such young $^{238}U/^{230}Th$ crystallisation ages are consistent with the (U–Th)/He eruption ages of ~45 ka, and lend independent support for a post-61 ka eruption age.

4.2. Implications for the MIS correlations and volcanism in the TVZ

The Rotoehu tephra forms a regionally important stratigraphic marker in New Zealand and the SW Pacific, and its age is critical for paleoclimatic reconstructions because there is little datable material in the ~40–70 ka time interval. The age of 61 ± 1.4 ka proposed by Wilson et al. (2007) would place the eruption very close to the MIS 4/3 stadial–interstadial transition which is dated at ~59.1 ka on the basis of orbitally tuned oxygen isotope records from marine sediments and ice cores from Greenland and Antarctica (Martinson et al., 1987; Grootes et al., 2001; Shackleton et al., 2004). Given that the age of ~59.1 ka is subject to uncertainties inherent to ice-core geochronology (e.g., Blunier et al., 1998), Wilson et al. (2007) suggested that the Rotoehu tephra could be a more precise chronostratigraphic marker for the MIS 4/3 boundary. However, the new (U–Th)/He and ^{14}C age data for the age of the Rotoiti eruption (~45 ka) places the timing of eruption within the MIS 3 interstadial (~59.1–29.0 ka), well above the MIS 4/3 boundary. This is consistent with palynological evidence of an extended moist temperate period before the eruption, that followed a cold to warm transition (Shane and Sandiford, 2003).

The Rotoehu tephra layer is also an important anchor-point in the tephrochronological record of the New Zealand region. At least 68 TVZ silicic eruptions have been recognized in sediments above the tephra, and some of them have been dated on the basis of relative position to the Rotoehu tephra (Lowe, 2011). Thus, the age of the Rotoehu tephra has implications for the frequency of eruptions from the concurrently active Taupo and Okataina volcanic centres. Adopting the age of ~45 ka instead of ~61 ka would imply higher magma production rates and eruption frequency. For instance, an age of ~45 ka would indicate there was only a brief hiatus between the caldera collapse associated with the Rotoiti (=Rotoehu) eruption and the subsequent intra-caldera plinian eruptions of the Mangaone Subgroup loosely dated at ~45–30 ka (Jurado-Chichay and Walker, 2000). Similarly, some post-Rotoehu tephra deposits from Taupo volcano would be younger than proposed (Wilson et al., 2009) because their ages are partly derived from that of Rotoehu tephra. Adopting an age of 45 ka for the Rotoiti eruption, the average magma eruption rate for the TVZ shifts from 12.8 $km^3\ kyr^{-1}$ (=total dry rock equivalent volume of lava erupted per kyr) proposed by Wilson et al. (2009) to 17.4 $km^3\ kyr^{-1}$. Thus, we suggest that volcanological and paleoclimate interpretations based on the age of 61 ka have to be revised in the light of the younger age for the Rotoiti/EQF eruptions presented here.

5. Conclusions

Combined $^{238}U/^{230}Th$ disequilibrium and (U–Th)/He dating of zircon from Rotoiti and EQF deposits revealed the ages of $45.1(7) \pm 3.3$ ka and $45.1(6) \pm 2.9$ ka, respectively. These results are in excellent agreement with new and published high-precision ^{14}C data bracketing the age of the Rotoiti eruption between 44.8 ± 0.3 and 47.5 ± 2.1 ka cal BP and demonstrate the consistency between independent radiometric methods. The statistically insignificant difference between the (U–Th)/He ages for the two eruptions provides the first radiometric evidence for a brief ($\ll$1000 yrs) hiatus between them, as inferred from field exposures. The new ages are consistent with other independent determinations that have previously been questioned, including ^{14}C, OSL, palynology, stratigraphic, and other constraints. The (U–Th)/He ages are significantly younger than the age of 61.0 ± 1.4 ka, principally constrained by a single obsidian $^{40}Ar/^{39}Ar$ age of a glassy lava overlying the tephra (Wilson et al., 2007). The new eruption ages imply more frequent eruptive recurrence for the TVZ and qualify the widespread Rotoehu tephra to be used as a chronostratigraphic marker for MIS 3 in paleoenvironmental correlation studies. This study highlights the potential of the combined $^{238}U/^{230}Th$ disequilibrium and (U–Th)/He zircon dating technique for deposits that are close to or beyond the reach of ^{14}C or lack optimal materials for accurate and precise $^{40}Ar/^{39}Ar$ dating.

Acknowledgements

We thank B.J. McDonald (CSIRO) for the assistance with zircon dissolution, C. Scadding and A. Thomas (TSW Analytical) for assistance with ICP-MS analyses. Brent Alloway collected and kindly provided the Pouto 2 samples and stratigraphy of the site. Oscar M. Lovera developed the MCHeCalc code. C. Bronk Ramsey (Oxford University) assisted with developing the Tau boundary OxCal model. MD thanks D. Lowe (The University of Waikato) for sharing valuable information on tephrochronology of New Zealand. The ion microprobe facility at UCLA is partly supported by a grant from the Instrumentation and Facilities Program, Division of Earth Sciences, National Science Foundation. Two anonymous reviewers provided valuable comments.

Appendix A. Supporting information

Supplementary data associated with this article can be found in the online version at http://dx.doi.org/10.1016/j.epsl.2012.06.041.

References

Allan, A.S.R., Baker, J.A., Carter, L., Wysoczanski, R.J., 2008. Reconstructing the Quaternary evolution of the world's most active silicic volcanic system: insights from an similar to 1.65 Ma deep ocean tephra record d from Taupo Volcanic Zone. New Zealand. Quat. Sci. Rev 27, 2341–2360.

Blondes, M.B., Reiners, P.W., Edwards, B.R., Biscontini, A.E., 2007. Dating young basalts by (U–Th)/He on xenolithic zircons. Geology 35, 17–20.

Blunier, T., Chappellaz, J., Schwander, J., Dallenbach, A., Stauffer, B., Stocker, T.F., Raynaud, D., Jouzel, J., Clausen, H.B., Hammer, C.U., Johnsen, S.J., 1998. Asynchrony of Antarctic and Greenland climate change during the Last Glacial period. Nature 394, 739–743.

Bronk Ramsey, C., 2009. Bayesian analysis of radiocarbon dates. Radiocarb 51, 337–360.

Bronk Ramsey, C., 2010. OxCal progam v4.1.7. Available at ⟨http://c14.arch.oxac.uk/oxcal.html⟩.

Cassata, W.S., Singer, B.S., Liddicoat, J.C., Coe, R.S., 2010. Reconciling discrepant chronologies for the geomagnetic excursion in the Mono Basin, California: insights from new $^{40}Ar/^{39}Ar$ dating experiments and a revised relative paleointensity correlation. Quat. Geochron 5, 533–543.

Charlier, B., Zellmer, G., 2000. Some remarks on U–Th mineral ages from igneous rocks with prolonged crystallization histories. Earth Planet. Sci. Lett 183, 457–469.

Charlier, B.L.A., Peate, D.W., Wilson, C.J.N., Lowenstern, J.B., Storey, M., Brown, S.J.A., 2003. Crystallisation ages in coeval silicic magma bodies; $^{238}U–^{230}Th$ disequilibrium evidence from the Rotoiti and Earthquake Flat eruption deposits, Taupo volcanic zone, New Zealand. Earth Planet. Sci. Lett. 206, 3–4.

Charlier, B.L.A., Wilson, C.J.N., 2010. Chronology and evolution of caldera-forming and post-caldera magma systems at Okataina Volcano, New Zealand from zircon U–Th model-age spectra. J. Petrol 51 (5), 1121–1141.

Chen, Y., Smith, P.E., Evensen, N.M., York, D., Lajoie, K.R., 1996. The edge of time: dating young volcanic ash layers with the ^{40}Ar-^{39}Ar laser probe. Science 274 (5290), 1176–1178.

Esser, R.P., McIntosh, W.C., Heizler, M.T., Kyle, P.R., 1997. Excess argon in melt inclusions in zero-age anorthoclase feldspar from Mt. Erebus, Antarctica, as revealed by the $^{40}Ar/^{39}Ar$ method. Geochim. Cosmochim. Acta 61 (18), 3789–3801.

Evans, N.J., Byrne, J.P., Keegan, J.T., Dotter, L.E., 2005. Determination of uranium and thorium in zircon, apatite, and fluorite: application to laser (U–Th)/He thermochronology. J. Anal. Chem. 60 (12), 1159–1165.
Farley, K.A., 2002. (U–Th)/He dating: techniques, calibrations, and applications. Mineral. Soc. Am. Rev. Mineral. Geochem. 47, 819–844.
Farley, K.A., Kohn, B.P., Pillans, B., 2002. The effects of secular disequilibrium on (U–Th)/He systematics and dating of Quaternary volcanic zircon and apatite. Earth Planet. Sci. Lett 201 (1), 117–125.
Farley, K.A., Wolf, R.A., Silver, L.T., 1996. The effects of long alpha-stopping distances on (U–Th)/He ages. Geochim. Cosmochim. Acta 60 (21), 4223–4229.
Foland, K.A., Fleming, T.H., Heimann, A., Elliot, D.H., 1993. Potassium-argon dating of fine-grained basalts with massive Ar loss: Application of the $^{40}Ar/^{39}Ar$ technique to plagioclase and glass from the Kirkpatrick Basalt. Antarctica. Chem. Geol 107 (1–2), 173–190.
Froggatt, P.C., Lowe, D.J., 1990. A review of late Quaternary silicic and some other tephra formations from New Zealand: their stratigraphy, nomenclature, distribution, volume, and age. N. Z. J. Geol. Geophys 33, 89–109.
Grant-Taylor, T.L., Rafter, T.A., 1971. New Zealand radiocarbon age measurements - 6. N. Z. J. Geol. Geophys 14, 364–402.
Grootes, P.M., Steig, E.J., Stuiver, M., Waddington, E.D., Morse, D.L., Nadeau, M.-J., 2001. The Taylor Dome Antarctic ^{18}O record and globally synchronous changes in climate. Quat. Res 56, 289–298.
Hogg, A.G., Fifield, L.K., Turney, C.S.M., Palmer, J.G., Galbraith, R., Baillie, M.G.K., 2006. Dating ancient wood by high-sensitivity liquid scintillation counting and accelerator mass spectrometry-Pushing the boundaries. Quat. Geochron 1 (4), 241–248.
Hogg, A.G., Keith Fifield, L., Palmer, J.G., Turney, C.S.M., Galbraith, R., 2007. Robust radiocarbon dating of wood samples by high-sensitivity liquid scintillation spectroscopy in the 50–70 kyr age range. Radiocarb 49, 379–391.
Hora, J.M., Singer, B.S., Jicha, B.R., Beard, B.L., Johnson, C.M., de Silva, S., Salisbury, M., 2011. Volcanic biotite-sanidine $^{40}Ar/^{39}Ar$ age discordances reflect Ar partitioning and pre-eruption closure in biotite. Geology 38 (10), 923–926.
Jurado-Chichay, Z., Walker, G.P.L., 2000. Stratigraphy and dispersal of the Mangaone Subgroup pyroclastic deposits, Okataina Volcanic Centre, New Zealand. J. Volcanol. Geotherm. Res. 104, 319–383.
Kaneoka, I., 1972. The effect of hydration on the K/Ar ages of volcanic rocks. Earth Planet. Sci. Lett 14 (2), 216–220.
Lian, O., Shane, P., 2000. Optical dating of paleosols bracketing the widespread Rotoehu tephra, North Island. New Zealand Quat. Sci. Rev. 19, 1649–1662.
Lowe, D., 2011. Tephrochronology and its application: A review. Quat. Geochron 6 (2), 107–153.
Lowe, D.J., Hogg, A.G., 1995. Age of the Rotoehu ash. N. Z. J. Geol. Geophys 38, 399–402.
Ludwig, K.R., 2003. Isoplot/Ex version 3.41, a geochronological toolkit for Microsoft Excel. Berkeley Geochronology Center Special Publication, 4.
Mahon, K.I., 1996. The new "York" regression; application of an improved statistical method to geochemistry. Int. Geol. Rev. 38, 293–303.
Martinson, D.G., Pisias, N.G., Hays, J.D., Imbrie, J., Moore, T.C., Shackleton, N.J., 1987. Age dating and the orbital theory of the Ice Ages: development of a high-resolution 0 to 300,000-year chronostratigraphy. Quat. Res 27, 1–29.
McCormac, F.G., Reimer, P.J., Hogg, A.G., Higham, T.F.G., Baillie, M.G.L., Palmer, J.G., Stuiver, M., 2002. Calibration of the radiocarbon time scale for the Southern Hemisphere AD 1850–950. Radiocarb 44 (3), 641–651.
McDougall, I., Harrison, T.M., 1998. Geochronology and Thermochronology by the $^{40}Ar/^{39}Ar$ Method. Clarendon Press, Oxford, UK.
McDougall, I., Polach, H.A., Stipp, J.J., 1969. Excess radiogenic argon in young subaerial basalts from the Auckland volcanic field, New Zealand. Geochim. Cosmochim. Acta 33, 1485–1520.
Molloy, C., Shane, P., Nairn, I., 2008. Pre-eruption thermal rejuvenation and stirring of a partly crystalline rhyolite pluton revealed by the Earthquake Flat Pyroclastics deposits. N. Z. J. Geol. Soc 165 (1), 435–447.
Molloy, C., Shane, P., Augustinus, P., 2009. Eruption recurrence rates in a basaltic volcanic field based on tephra layers in maar sediments; implications for hazards in the Auckland volcanic field. Geol. Soc. Am. Bull 121, 11–12.
Morgan, L.E., Renne, P.R., Taylor, R.E., Wolde-Gabriel, G., 2009. Archaeological age constraints from extrusion ages of obsidian: Examples from the Middle Awash. Ethiopia. Quat. Geochron 4 (3), 193–203.
Nairn, I.A., 2002. Geology of the Okataina Volcanic Centre. Institute of Geological & Nuclear Sciences Geological Map 25. Institute of Geological & Nuclear Sciences, Lower Hutt, New Zealand.
Nairn, I.A., Kohn, B.P., 1973. Relation of the Earthquake Flat Breccia to Rotoiti Breccia, central North Island, New Zealand. N. Z. J. Geol. Geophys 16, 269–279.
Nilsson, A., Muscheler, R., Snowball, I., Aldahan, A., Possnert, G., Augustinus, P., Atkin, D., Stephens, T., 2011. Multi-proxy identification of the Laschamp geomagnetic field excursion in Lake Pupuke, New Zealand. Earth Planet. Sci. Lett. 311 (1–2), 155–164.
Paces, J.B., Miller Jr., J.D., 1993. Precise U-Pb Ages of Duluth Complex and Related Mafic Intrusions, Northeastern Minnesota: Geochronological Insights to Physical, Petrogenetic, Paleomagnetic, and Tectonomagmatic Processes Associated With the 1.1 Ga Midcontinent Rift System. J. Geophys. Res 98 (13) 997-14.
Pullar, W.A., Birrell, K.S., 1973. Age and distribution of late Quaternary pyroclastic and associated cover deposits of the Rotorua and Taupo Area, North Island, New Zealand, Parts I and II. Maps of isopachs and volumes of tephra and subsurface loess, central North Island, New Zealand 1: 1,000,000, New Zealand Soil Survey Report, 1, NZDSIR, Wellington, New Zealand.
Reimer, P.J., Baillie, M.G.L., Bard, E., Bayliss, A., Beck, J.W., Blackwell, P.G., Bronk Ramsey, C., Buck, C.E., Burr, G.S., Edwards, R.L., Friedrich, M., Grootes, P.M., Guilderson, T.P., Hajdas, I., Heaton, T.J., Hogg, A.G., Hughen, K.A., Kaiser, K.F., Kromer, B., McCormac, F.G., Manning, S.W., Reimer, R.W., Richards, D.A., Southon, J.R., Talamo, S., Turney, C.S.M., van der Plicht, J., Weyhenmeyer, C.E., 2009. IntCal09 and Marine09 radiocarbon age calibration curves, 0–50,000 years cal BP. Radiocarb 51, 1111–1150.
Reiners, P.W., Spell, T.L., Nicolescu, S., Zanetti, K.A., 2004. Zircon (U–Th)/He thermochronometry: He diffusion and comparisons with $^{40}Ar/^{39}Ar$ dating. Geochim. Cosmochim. Acta 68 (8), 1857–1887.
Renne, P.R., Sharp, W.D., Deino, A.L., Orsi, G., Civetta, L., 1997. $^{40}Ar/^{39}Ar$ dating into the historical realm: calibration against pliny the younger. Science 277 (5330), 1279–1280.
Rosman, K.J.R., Taylor, P.D.P., 1998. Isotopic compositions of the elements 1997. Pure and Appl. Chem. 70 (1), 217–222.
Santos, G.M., Bird, M.I., Pillans, B., Fifield, L.K., Alloway, B.V., Chappell, J., Hausladen, P.A., Arneth, A., 2001. Radiocarbon dating of wood using different pre-treatment procedures: application to the chronology of Rotoehu ash, New Zealand. Radiocarb 43, 239–248.
Santos, G.M., Moore, R.B., Southon, J.R., Griffin, S., Hinger, E., Zhang, D., 2007. AMS ^{14}C sample preparation at the KCCAMS/UCI Facility: status report and performance of small samples. Radiocarb 49 (2), 255–269.
Schmitt, A.K., 2007. Ion microprobe analysis of $(^{231}Pa)/(^{235}U)$ and an appraisal of protactinium partitioning in igneous zircon. Am. Mineral 92 (4), 691–694.
Schmitt, A.K., 2011. Uranium series accessory crystal dating of magmatic processes. Ann. Rev. Earth Planet. Sci 39, 321–349.
Schmitt, A.K., Stockli, D.F., Hausback, B.P., 2006. Eruption and magma crystallization ages of Las Tres Vírgenes (Baja California) constrained by combined $^{230}Th/^{238}U$ and (U–Th)/He dating of zircon. J. Volcanol. Geoth. Res 158 (3–4), 281–295.
Schmitt, A.K., Stockli, D.F., Lindsay, J.M., Robertson, R., Lovera, O.M., Kislitsyn, R., 2010. Episodic growth and homogenization of plutonic roots in arc volcanoes from combined U–Th and (U–Th)/He zircon dating. Earth Planet. Sci. Lett. 295 (1–2), 91–103.
Schmitt, A.K., Danišík, M., Evans, N.J., Siebel, W., Kiemele, E., Aydin, F., Harvey, J.C., 2011. Acigöl rhyolite field, Central Anatolia (part 1): high-resolution dating of pre-eruptive zircon residence and rhyolite eruption episodes. Contrib. Mineral. Petrol. 162 (6), 1215–1231.
Shackleton, N.J., Fairbanks, R.G., Chiu, T.-C., Parrenin, F., 2004. Absolute calibration of the Greenland time scale: implications for Antarctic time scales and for $D^{14}C$. Quat. Sci. Rev. 23, 1513–1522.
Shane, P., 2000. Tephrochronology: A New Zealand case study. Earth-Sci. Rev. 49, 223–259.
Shane, P., Sandiford, A., 2003. Paleovegetation of Marine Isotope Stages 4 and 3 in northern New Zealand and the age of the widespread Rotoehu tephra. Quat. Res 59, 420–429.
Shane, P., Nairn, I.A., Smith, V.C., 2005. Magma mingling in the ~50 ka Rotoiti eruption from Okataina Volcanic Centre: implications for geochemical diversity and chronology of large volume rhyolites. J. Volcanol. Geoth. Res 139, 295–313.
Shane, P., Sikes, E.L., Guilderson, T.P., 2006. Tephra beds in deep-sea cores off northern New Zealand: implications for the history of Taupo Volcanic Zone, Mayor Island and White Island volcanoes. J. Volcanol. Geoth. Res 154, 276–290.
Singer, B.S., Wijbrans, J.R., Nelson, S.T., Pringle, M.S., Feeley, T.C., Dungan, M.A., 1998. Inherited argon in a Pleistocene andesite lava: $^{40}Ar/^{39}Ar$ incremental-heating and laser fusion analyses of plagioclase. Geology 26, 427–430.
Spell, T.L., Smith, E.I., Sanford, A., Zanetti, K.A., 2001. Systematics of xenocrystic contamination: preservation of discrete feldspar populations at McCullough Pass Caldera revealed by $^{40}Ar/^{39}Ar$ dating. Earth Planet. Sci. Lett. 190, 153–165.
Storm, S., Shane, P., Schmitt, A.K., Lindsay, J.M., 2011. Decoupled crystallization and eruption histories of the rhyolite magmatic system at Tarawera volcano revealed by zircon ages and growth rates. Contrib. Mineral Petrol , http://dx.doi.org/10.1007/s00410-011-0682-8.
Thompson, B.N., 1968. Age of Rotoiti Breccia. N.Z. J. Geol. Geophys 11 (5), 1189–1191.
Villa, I.M., 1991. Excess argon in potassic volcanites. Schweiz. Mineral. Petrogr. Mitt. 71, 205–209.
Walker, D.A., McDougall, I., 1982. $^{40}Ar/^{39}Ar$ and K/Ar dating of altered glassy rocks: the Dabi Volcanics. P.N.G. Geochim. Cosmochim. Acta 46, 2181–2190.
Walter, R.C., Manega, P.C., Hay, R.L., 1991. Laser-fusion Ar^{40}/Ar^{39} dating of bed I, Olduvai-Gorge, Tanzania. Nature 354, 145–149.
Wiedenbeck, M., Alle, P., Corfu, F., Griffin, W.L., Meier, M., Oberli, F., von Quadt, A., Roddick, J.C., Spiegel, C., 1995. Three natural zircon standards for U–Th–Pb, Lu–Hf, trace element and REE analyses. Geostand. Newslett 19 (1), 1–23.
Wilson, C.J.N., Houghton, B.F., Lanphere, M.A., Weaver, S.D., 1992. A new radiometric age estimate for the Rotoehu Ash from Mayor Island volcano. New Zealand J. Geol. Geophys 35, 371–374.
Wilson, C.J.N., Rhoades, D.A., Lanphere, M.A., Calvert, A.T., Houghton, B.F., Weaver, S.D., Cole, J.W., 2007. A multiple-approach radiometric age estimate for the Rotoiti and Earthquake Flat eruptions, New Zealand, with implications for the MIS 4/3 boundary. Quat. Sci. Rev. 26, 1861–1870.
Wilson, C.J.N., Gravley, D.M., Leonard, G.S., Rowland, J.V., 2009. Volcanism in the central Taupo Volcanic Zone, New Zealand: tempo, styles and controls. In: Thordarson, T., Self, S., Larsen, G., Rowland, S.K., Hoskuldsson, A. (Eds.), Studies in Volcanology: The Legacy of George Walker. Special Publications of IAVCEI, 2. Geological Society, London, pp. 225–247.